


Piotr Górski  orcid.org/0000-0001-9355-3410
p.gorski@po.opole.pl

Marcin Tataro  orcid.org/0000-0002-4437-7155
Department of Roads and Bridges, Opole University of Technology, Poland

Stanislav Pospíšil  orcid.org/0000-0002-5927-7587

Sergej Kuznetsov
Institute of Theoretical and Applied Mechanics, Academy of Sciences of the Czech Republic

MODEL INVESTIGATIONS OF THE AERODYNAMIC COEFFICIENTS OF ICED CABLES IN CABLE-STAYED BRIDGES

BADANIA MODELOWE WSPÓŁCZYNNIKÓW AERODYNAMICZNYCH OBLODZONEGO CIĘGNA MOSTU PODWIESZONEGO

Abstract

This paper presents the wind tunnel investigations of the mean aerodynamic coefficients of the stationary iced model in cable-stayed bridges. The investigations were performed in a Climatic Wind Tunnel Laboratory at the Czech Academy of Sciences in Telč. The icing of the inclined cable model was made experimentally. The shape of the iced model was mapped by a photogrammetry method. The new iced cable model was made by using a 3D printer. The aerodynamic drag, lift and moment coefficients were determined with respect to three principal angles of wind attack within the range of the Reynolds number between $2.5 \cdot 10^4$ and $13.6 \cdot 10^4$ at a turbulence intensity of 5%. It was found that the drag coefficient values of the iced cable model are higher than for a circular smooth cylinder. The obtained results could constitute a basis to formulate a mathematical description of the wind load acting on the iced cables of cable-supported bridges.

Keywords: bridge cable, ice accretion, angle of wind attack, aerodynamic coefficient

Streszczenie

W pracy podano sposób i wyniki badań statycznych współczynników aerodynamicznych nieruchomego modelu oblodzonego cięgna mostu podwieszonego. Badania wykonano w tunelu aerodynamicznym Laboratorium Czeskiej Akademii Nauk w Telči. Zrealizowano doświadczalne oblodzenie nachylonego modelu cięgna. Otrzymane oblodzenie zarejestrowano metodą fotogrametrii. Wykonano nowy model oblodzonego cięgna metodą druku 3D. Współczynniki aerodynamiczne wyznaczono przy trzech podstawowych kierunkach napływającego powietrza w zakresie liczby Reynoldsa od $2,5 \cdot 10^4$ do $13,6 \cdot 10^4$ i przy średniej intensywności turbulencji powietrza 5%. Stwierdzono, że wartości współczynnika oporu aerodynamicznego modelu oblodzonego cięgna są większe w porównaniu do wartości otrzymanych dla cylindra. Otrzymane wyniki mogą stanowić podstawę do sformułowania matematycznego opisu modelu obciążenia wiatrem oblodzonych cięgien mostowych.

Słowa kluczowe: cięgna mostowe, oblodzenie, kąt napływu powietrza, współczynnik aerodynamiczny

1. Introduction

The ice accretion on the slender bridge elements, e.g. the bridge cables, has a significant influence on the flow field around the cables and their aerodynamics and can lead to a much larger amplitude of cable vibrations under wind action than in the case of a dry cable. This statement was confirmed on the basis of the vibration measurements of the iced hanger of the Great Belt Suspension Bridge in Denmark due to the wind, described in the paper [6]. The respective vibration amplitudes of the iced hanger, recorded on March 29, 2001, were approximately 1.4 m in the across-wind direction and approximately 1.0 m in the along-wind direction. It is notable that such large vibration amplitudes were not observed in the case of a dry hanger, i.e. without ice. For this reason, the investigation of the influence of ice on the aerodynamics of the bridge cables is a very important issue when considering the safety of cable-supported bridges.

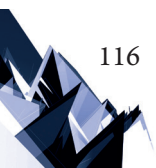
In the case of an asymmetric airflow around the iced circular cable, an asymmetric distribution of the wind pressure on its surface may occur. For this reason, three aerodynamic coefficients, i.e. drag, lift and moment coefficients should be considered under ice conditions. The values of these coefficients depend on the shape of the ice, wind velocity, turbulence intensity of the airflow, the angle of the wind attack and the character of the flow field in the wake behind the cable. Moreover, an aeroelastic instability of the iced cable known as the galloping instability may occur if the specific criteria proposed by den Hartog [8] are met. This phenomenon is related to the change in the value of the aerodynamic coefficients depending on the angle of the wind attack [4]. The knowledge of the aerodynamic coefficients could be the basis to formulate the mathematical description of the wind load acting on the iced cables of cable-supported bridges in order to predict the cable response due to the wind.

It should be noted that the literature concerning the influence of ice on the aerodynamics of the cables of cable-stayed bridges is relatively poor. Therefore, currently, it is very advisable and valuable to conduct further studies in this field. Some contemporary achievements are presented in the papers [1, 2, 5, 7, 12].

This paper deals with the method and results of wind tunnel investigations of mean aerodynamic coefficients, i.e. drag, lift and moment coefficients of the iced cable model of cable-stayed bridges with respect to three principal angles of wind attack. The tests were performed within the range of the *Reynolds* number (Re) between $2.5 \cdot 10^4$ and $13.6 \cdot 10^4$ at a mean turbulence intensity of 5%. The experiments were carried out in the Climatic Wind Tunnel Laboratory of the Czech Academy of Sciences in Telč.

2. The icing process and the preparation of the iced cable model for aerodynamic investigations

The experimental icing process of a cable section model was conducted in the climatic chamber of the closed-return wind tunnel of CET ITAM [9]. The cable model was made of polyvinylchloride (PVC), whose surface is similar to the surface of a cable cover made of high-density polyethylene (HDPE). The 2.5 m long pipe-shaped model with



a circular cross-section measuring 0.160 m in diameter was inclined at an angle of 30° in the vertical plane, and at an angle of 60° in the horizontal plane with respect to the wind direction. The suspension of the cable model in the climatic section is shown in Fig. 1a. The icing process was performed during a 40 minute time period at an average temperature of slightly below 0°C, a mean free stream velocity of 2.8 m/s with rainy conditions created using rain sprinklers with diameter heads of 2.8 mm. The probability of the ideal meteorological conditions for icing bridge cables occurring naturally is not so high. Roldsgaard et al. [10], estimated that conditions conducive to icing occur for a total of about 96 hours per year, based on monitoring data from the vicinity of the Øresund Bridge in Denmark, using the Bayesian Probabilistic Network.

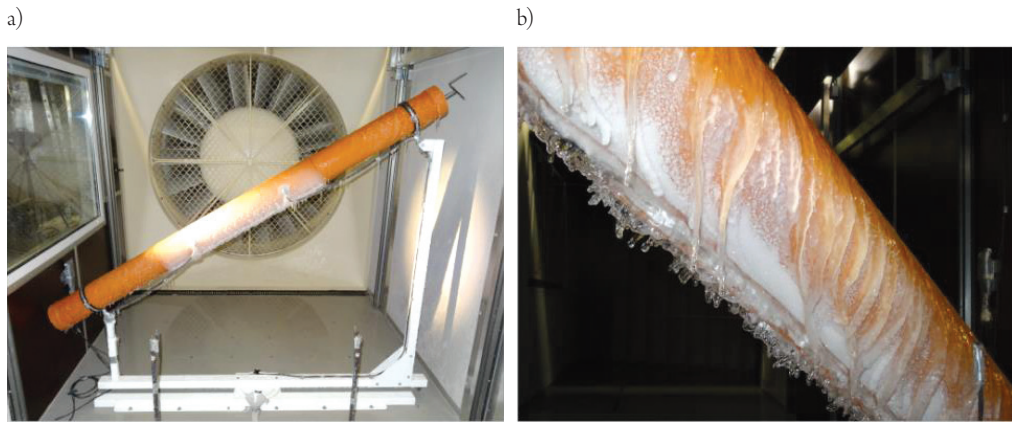


Fig. 1. (a) View of the fixation of the cable model in a special frame in the climatic section during the icing process, and (b) view of the final icing effect from the bottom side of the cable model

The final ice shape on the bottom side of the cable model featured characteristically irregular ice ribs with rounded edges and a relatively maximal surface roughness of 18% (Fig. 1b). On the upper part of the cross-section of the model, the ice was similar to a circular shape with a minimal surface roughness of 0.73%. The relative surface roughness was related to the cable diameter and was measured taking into account only the dominant (most prominent) peaks, which are, in case of the considered model, caused by the irregularly iced cross-section. The variable cross-section of the cable with ice became strongly nonsymmetrical with average dimensions of 0.192 m in height and 0.181 m in width.

Immediately after the icing process, the shape of the iced cable model was captured by a photogrammetry method. Using a numerical image analysis, a three-dimensional (3D) numerical model of the iced cable was obtained (Fig. 2a). For aerodynamic investigations the new iced cable model, shown in Fig. 2b, was made of polylactide plastic at a scale of 1:1.6 using a 3D printing procedure. The average outer dimensions of the model cross-section were 0.120 m in height and 0.113 m in width while the model length was 0.435 m. The detailed descriptions of the icing process, the final icing effect and preparation of the new iced cable model for the wind tunnel investigations are presented in a previous paper [7].

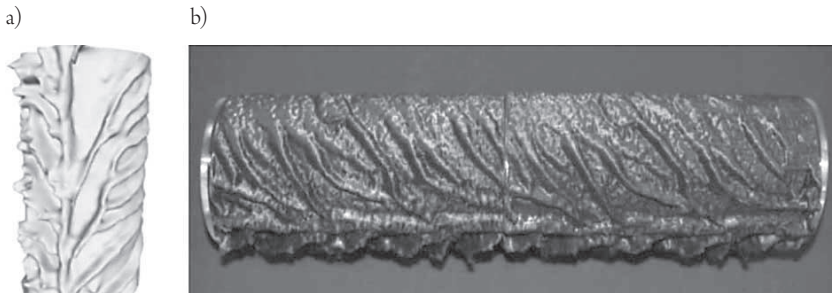


Fig. 2. (a) Three-dimensional numerical model of the iced cable in a scale 1:1, and (b) iced cable model created using a 3D printing method for the aerodynamic investigations

3. Experimental set-up of aerodynamic investigations

The tests were conducted in the aerodynamic section of the wind tunnel. This section has a rectangular cross-section with a height of 1.8 m, a width of 1.9 m, and a length of 11.0 m. The aerodynamic investigations of the iced cable model were performed with respect to determining three mean aerodynamic coefficients, i.e. drag, lift and moment coefficients as functions of Re . The tests were conducted for three principal configurations of the ice cable model in relation to the flow direction which are presented in Fig. 3. In this figure, the reference dimension d defined as the span-averaged outer dimension of each model configuration perpendicular to the airflow direction is shown.

Measurements of aerodynamic forces were made using the three-component aerodynamic force balance based on the electric resistant wire strain gauges which are able to measure drag, lift and moment forces, simultaneously. Six strain gauges of type Megatron KM102 were used with an operative range from 0 to 100 N at a temperature range of -10°C to 40°C , and with a declared nonlinearity of the sensors of 0.04%. Strain gauges were connected to the Dewetron acquisition system type DEWE-801-TR.

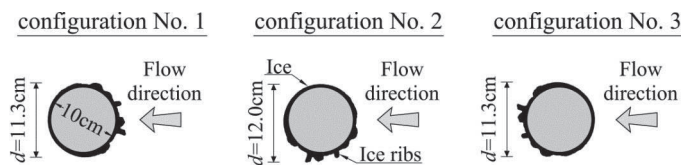


Fig. 3. Model configurations and the reference dimension d defined as the span-averaged outer dimension of the model, perpendicular to the airflow direction considered for the aerodynamic investigations

The sectional model was fixed motionlessly (in both support points the movement of the model was blocked in each direction) with the force balance in a horizontal position at a level of 69.3 cm above the floor of the aerodynamic section, crosswise to the airflow. Two sides of the force balance frame were equipped with plexi-glass end-plates to ensure a two-dimensional flow around the model. The sketch of the experimental set-up in the aerodynamic chamber is shown in Fig. 4.

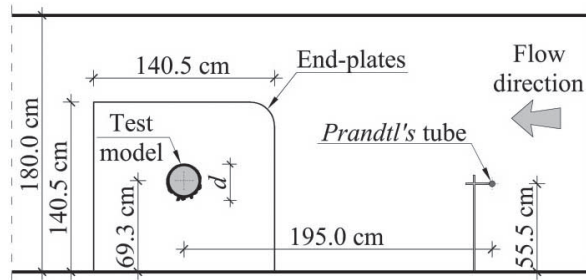


Fig. 4. Sketch of the experimental set-up in the aerodynamic section (view along the section)

The aerodynamic coefficients were investigated according to the following methodology. During the tests, the free stream velocity \bar{u}^P was measured by *Prandtl's* tube placed upstream of the model centerline at a distance of 195 cm, i.e. in front of the force balance, and at a level of 55.5 cm above the floor of the aerodynamic section. Simultaneously, three radial forces acting on the iced model, i.e. drag, lift and moment forces were measured on both ends of the model by the three-component aerodynamic force balance (Fig. 5). For each model configuration, three time series of measurements at each mean free stream velocity \bar{u}^P were made during the 60 s interval with a sampling rate of 100 Hz.

Due to the reduction of the flow area in the aerodynamic chamber by the presence of the force balance, the increase of the air flow velocity acting on the model between the end-plates of the balance, was observed as the blockage effect. In order to recognize the influence of this phenomenon on the test results, it was necessary to determine the reference wind velocity \bar{u}_{ref} acting on the test model, i.e. the wind velocity measured in the undisturbed flow in the vicinity of the front of the model, between the end-plates of the force balance.

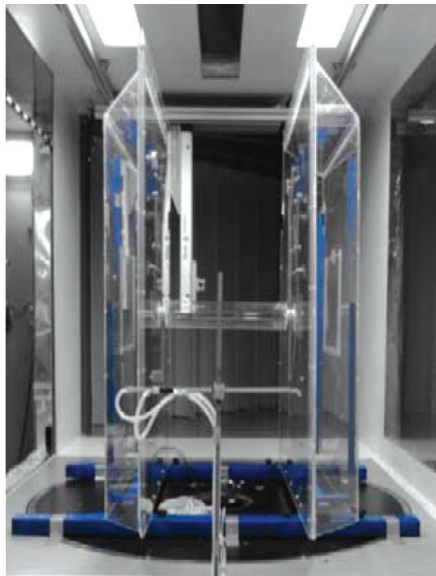


Fig. 5. View of the aerodynamic force balance in the aerodynamic section

The reference value of the wind velocity should be taken into consideration in the calculation of the aerodynamic coefficients of the iced model. For this purpose, the definition of the correction factor γ of the wind velocity was introduced in the following form:

$$\gamma = \frac{\bar{u}_{sr}^T}{\bar{u}^P}, \quad (1)$$

where: \bar{u}^P is the time-averaged free stream velocity upstream of the force balance, i.e. in the position of *Prandtl's* tube reference, and \bar{u}_{sr}^T is the time and span-averaged wind velocity along the longitudinal axis position of the test model in the undisturbed flow between the end-plates of the balance.

The time- and span-averaged wind velocity \bar{u}_{sr}^T was determined according to the formula:

$$\bar{u}_{sr}^T = \frac{\sum_{i=1}^n \bar{u}_i^T}{n}, \quad (2)$$

where \bar{u}_i^T is the time-averaged wind velocity recorded at the i -th measurement point along the longitudinal axis position of the test model, in the undisturbed flow between the end-plates of the force balance and n is the total number of measurement points.

In order to calculate the correction factor γ , the 30-second mean wind velocities \bar{u}^P and \bar{u}_i^T were measured by CTA (Constant Temperature Anemometry) sensors using two hot-wire anemometers simultaneously. During the tests, one reference CTA sensor was fixed in the position of the *Prandtl's* tube, while the second one was moved step by step from measurement point No. 1 to point No. 21. The locations of the measurement points were adjusted within a 2 cm distance along the longitudinal axis of the iced model. Fig. 6 depicts the locations of the measurement points along the longitudinal axis of the model between the end-plates of the balance. With every rearrangement of the rover CTA, i.e. at each measurement point, six series of measurements were performed at the free stream velocity \bar{u}^P from 5.0 m/s to 16.3 m/s.

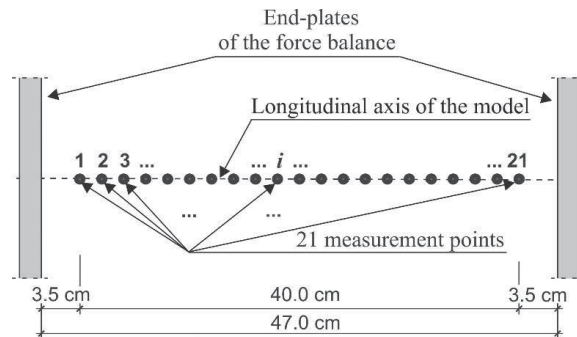


Fig. 6. Locations of measurement points along the longitudinal axis of the iced cable model between the end-plates of the force balance

Fig. 7 shows the measured distributions of time-averaged wind velocities \bar{u}_i^T along the iced model axis position for six various time-averaged free stream velocities \bar{u}^P . It should be noticed that streamwise velocity is not symmetrically distributed along the horizontal line over the width of the test section. This is possibly due to the flow separation and pressure drop in the cross-section of the closed-circuit wind tunnel as a result of the air flow through the ducts joined together at an angle of 90° [9].

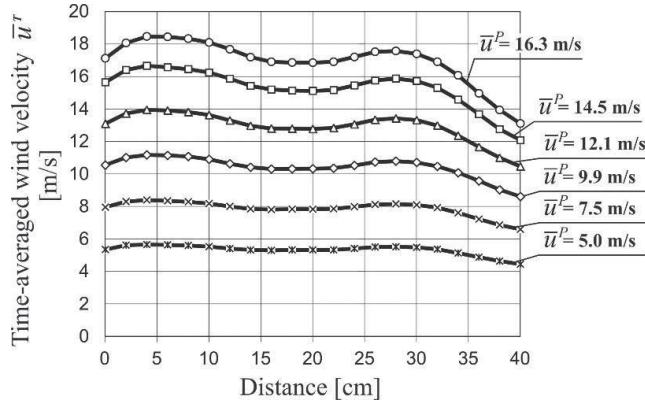


Fig. 7. Distributions of time-averaged wind velocities \bar{u}_i^T along the iced model axis position for six time-averaged free stream velocities \bar{u}^P

The values of correction factor γ corresponding to the mean free stream velocities \bar{u}^P within the range of 5.0 to 16.3 m/s were constant and were equal to $\gamma = 1.06$. It means that the blockage effect caused a 6% rise in \bar{u}_{sr}^T in comparison to \bar{u}^P .

One should be aware that the blockage ratio computed as the total surface area of the model as well as the end-plates of the force balance, projected normally to the free stream velocity, divided by the total area of the aerodynamic chamber cross-section, was about 15%. Therefore, in this case the correction factor γ including the blockage effects was crucial for the present study and was taken into account in the calculations of the mean aerodynamic coefficients.

The reference wind velocity \bar{u}_{ref} acting on the iced model was determined from the formula:

$$\bar{u}_{ref} = \bar{u}^P \cdot \gamma. \quad (3)$$

The Re values, corresponding to \bar{u}_{ref} , were evaluated according to the formula:

$$Re = \frac{\rho \cdot d \cdot \bar{u}_{ref}}{\mu}, \quad (4)$$

where: $\bar{u}_{ref} = 1.06 \cdot \bar{u}^P$,

$$\rho = \frac{P}{R \cdot T} \cdot 100 \quad (5)$$

is the air density, kg/m³; P is the atmospheric pressure of the air, hPa; $R = 287 \text{ m}^2/(\text{s}^2 \cdot \text{K})$ is the gas constant; T is the air temperature, °C,

$$\mu = \mu_0 \left(\frac{T}{T_0} \right)^{0.76} \quad (6)$$

is the dynamic viscosity of the air, Pa · s; $\mu_0 = 17.1 \cdot 10^{-6} \text{ Pa} \cdot \text{s}$, and $T_0 = 273 \text{ K}$.

During the tests, the airflow was modeled with a turbulence intensity of order 5%. In order to calculate accurate Re values, the actual air temperature T and the atmospheric pressure of the air P inside the aerodynamic section were measured continuously. During the tests, the mean air temperature was about 27°C and the atmospheric pressure was equal to 957 hPa. The investigations were carried out at twelve sequential free stream velocities in a range between 3.6 m/s and 18.9 m/s, corresponding to the twelve Re number regimes in the interval $Re = 2.5 \cdot 10^4$ to $13.6 \cdot 10^4$.

4. Experimental results

The mean aerodynamic coefficients, i.e. drag C_D , lift C_L and moment C_M coefficients were calculated regarding the measured, 60-second averaged aerodynamic forces acting on the total surface area of the test model, projected normally to the free stream velocity taking into account the reference wind velocity \bar{u}_{ref} . The aerodynamic coefficients were calculated according to the following formulas:

$$C_D = \frac{\bar{F}_D}{0.5 \cdot \rho \cdot \bar{u}_{ref}^2 \cdot d \cdot l}, \quad (7)$$

$$C_L = \frac{\bar{F}_L}{0.5 \cdot \rho \cdot \bar{u}_{ref}^2 \cdot d \cdot l}, \quad (8)$$

$$C_M = \frac{\bar{F}_M}{0.5 \cdot \rho \cdot \bar{u}_{ref}^2 \cdot d^2 \cdot l}, \quad (9)$$

where: \bar{F}_D , \bar{F}_L , \bar{F}_M are the 60-second averaged aerodynamic drag, lift and moment forces, respectively, d is the span-averaged outer dimension of the model perpendicular to the airflow direction (Fig. 3), and l is the length of the model equal to 0.435 m.

In order to validate the performance of the aerodynamic investigations, the tests for a circular smooth cylinder with a diameter of 10 cm were conducted first. In this case, the experimental set-up was arranged in the same manner as in the case of the iced cable model.

During the tests, Re was in the range from $2.8 \cdot 10^4$ to $13.2 \cdot 10^4$, i.e. within the subcritical range of Re for the circular smooth cylinder. Fig. 8a shows the measured mean aerodynamic drag force as a function of the reference wind velocity \bar{u}_{ref} , while Fig. 8b shows the mean drag coefficient as a function of Re for the circular smooth cylinder.

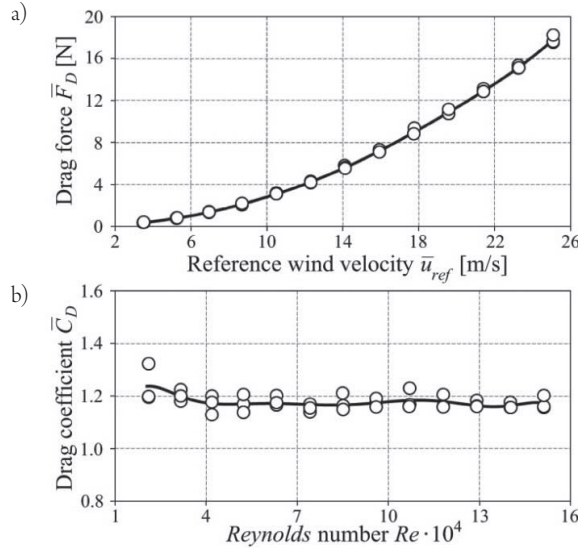


Fig. 8. (a) Variation of the mean aerodynamic drag force \bar{F}_D , with the reference wind velocity \bar{u}_{ref} , and (b) variation of the mean aerodynamic drag coefficient C_D with the Re number for the circular smooth cylinder

The obtained values of the aerodynamic drag coefficient C_D were changing from 1.13 to 1.22 for almost the entire range of Re that was studied. Only at a lowest value of $Re = 2.8 \cdot 10^4$, was the C_D coefficient slightly more than 1.3. Based on the results, it can be stated that the measured C_D values around 1.2 correspond well with the value reported by Schewe [11] and provided by the Eurocode Standard [3]. Thus, the preliminary results confirmed the validity of the adopted research methodology.

The mean values of each aerodynamic force and coefficient, obtained from three time series of measurements, were approximated and are shown as a continuous (for configuration No. 1), dashed (for configuration No. 2) and dotted (for configuration No. 3) lines in Figs 9, 10 and 11. The approximated values were taken further as the resulting values. Figs 9a, 10a and 11a depict the dependence of the measured and approximated mean aerodynamic forces, i.e. drag \bar{F}_D , lift \bar{F}_L , and moment \bar{F}_M , respectively, on the reference wind velocity \bar{u}_{ref} for three considered configurations of the ice cable model in relation to the flow direction. Figs 9b, 10b and 11b depict the dependence of the measured and approximated mean aerodynamic coefficients, i.e. drag C_D , lift C_L and moment C_M coefficients, respectively, on the Re number for three principal configurations of the ice cable model.

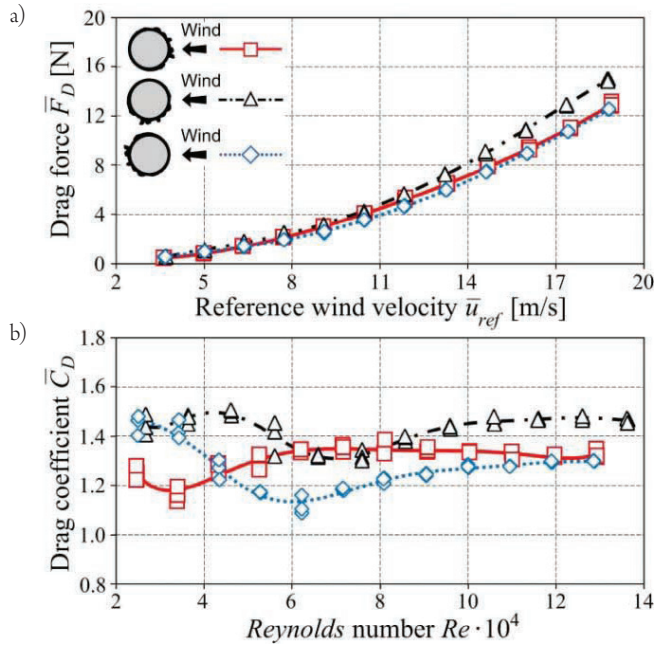


Fig. 9. (a) Mean aerodynamic drag force \bar{F}_D , versus the reference wind velocity \bar{u}_{ref} , and (b) mean aerodynamic drag coefficient C_D versus Re of the ice cable model for three principal angles of wind attack (configuration No.'s 1, 2 and 3)

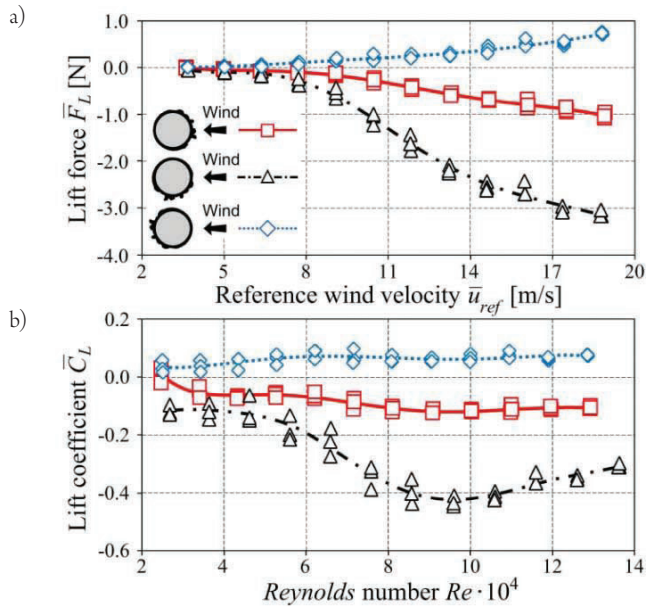


Fig. 10. (a) Mean aerodynamic lift force \bar{F}_L versus the reference wind velocity \bar{u}_{ref} , and (b) mean aerodynamic lift coefficient C_L versus Re of the ice cable model for three principal angles of wind attack (configuration No.'s 1, 2 and 3)

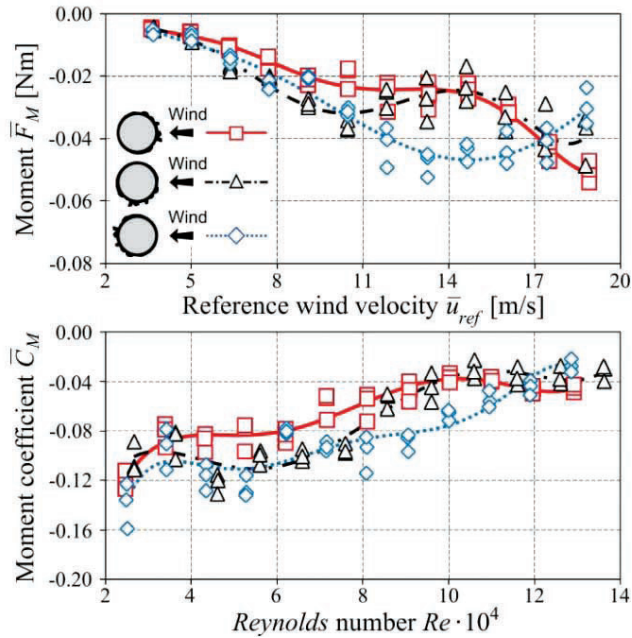


Fig. 11. (a) Mean aerodynamic moment \bar{F}_M versus the reference wind velocity \bar{u}_{ref} , and (b) mean aerodynamic moment coefficient \bar{C}_M versus Re of the ice cable model for three principal angles of wind attack (configuration No.'s 1, 2 and 3)

5. Concluding remarks

The experimental icing process of the inclined cable model of the cable-supported bridge was carried out in the Climatic Wind Tunnel Laboratory of the Czech Academy of Sciences in Telč. As a result of the icing process, the cross-section of the cable model became asymmetric and irregular with the rounded edges of the ice ribs accreted on the bottom side of the model and with a quasi-circular shape on its upper part. Then, it was clearly proved that the ice accretion on the cable model has a significant influence on the aerodynamic forces acting on the model. The airflow around the iced cable model is asymmetrical in relation to oncoming flow and there was an asymmetrical distribution of wind pressure on its surface. This phenomenon has been ascertained experimentally by measuring three components of the aerodynamic forces acting on the iced model. In the case of the circular cylinder, only the aerodynamic drag force is presented. Three mean aerodynamic coefficients, i.e. drag, lift and moment coefficients were investigated for the stationary iced cable model within the range of Re between $2.5 \cdot 10^4$ and $13.6 \cdot 10^4$. The aerodynamic investigations were conducted under the assumption that the mean wind direction during the icing process is independent of the wind direction during the investigations of aerodynamic coefficients. Therefore, the aerodynamic investigations were conducted with respect to three principal configurations of the model cross-section with respect to inflowing wind direction, namely for configuration No.'s 1, 2 and 3 (Fig. 3), each being perpendicular to the longitudinal axis of the cable model.

The determined values of the mean drag coefficient C_D for all considered model configurations depends on Re (Fig. 9b). For configuration No. 1 C_D varied in a range from 1.13 to 1.39. The lowest values of C_D were identified in the Re range of $2.5 \cdot 10^4$ and $4.3 \cdot 10^4$. In the remaining Re range, the C_D values changed slightly in the range from 1.26 to 1.39. For configuration No. 2, the C_D values were from 1.30 to 1.50 and the lowest values were in the range of Re from $5.6 \cdot 10^4$ and $8.6 \cdot 10^4$. $C_D = 1.2$ was used as a reference for the smooth circular cylinder and all the C_D values obtained for configuration No. 2 were higher than $C_D = 1.2$ by about 8% to 25%. In the case of configuration No. 3, the C_D values were within the range of 1.09 to 1.48, with the highest values for Re from $2.5 \cdot 10^4$ to $3.4 \cdot 10^4$. In the range of Re from $3.4 \cdot 10^4$ and $6.2 \cdot 10^4$, the C_D values decreased from 1.4 to 1.09. For Re greater than $6.2 \cdot 10^4$, C_D was slightly increased to 1.30.

The mean lift coefficient C_L determined for configuration No. 1 and 3 seems to be independent of Re in the range that was studied (Fig. 10b). For configuration No. 1, C_L varied in the range from 0.06 to -0.13 (the change of sign indicates the change in direction of the lift force acting on the model), while for configuration No. 3, C_L varied in the range from 0.03 to 0.10 for the entire range of Re that was studied. The highest absolute values of C_L were found in the case of configuration No. 2 within the range from -0.09 to -0.44 , however, the greatest values were in the range of Re from $7.6 \cdot 10^4$ to $12.6 \cdot 10^4$.

The mean moment coefficient C_M determined for all configurations strictly depends on Re (Fig. 11b). For all configurations, the C_M values increased slightly from -0.13 to -0.02 for the entire range of Re that was studied.

This research was financially supported by the CET sustainability project LO1219 (SaDeCET) of the Ministry of Education, Youth and Sport of the Czech Republic.

References

- [1] Demartino C., Koss H.H., Georgakis C.T., Ricciardelli F., *Effects of ice accretion on the aerodynamics of bridge cables*, Journal of Wind Engineering and Industrial Aerodynamics, Vol. 138, 2015, 98–119.
- [2] Demartino C., Ricciardelli F., *Aerodynamic stability of ice-accreted bridge cables*, Journal of Fluids and Structures, Vol. 52, 2015, 81–100.
- [3] Eurocode 1. *Action on structures – part 1–4: General action – Wind action*, 2009.
- [4] Flaga A., Michałowski T., *Zagadnienia aerodynamiki cięgien w mostach podwieszonych*, Inżynieria i Budownictwo, Vol. 6, 1997, 316–321.
- [5] Gjelstrup H., Georgakis C.T., Larsen A., *An evaluation of iced bridge hanger vibrations through wind tunnel testing and quasi-steady theory*, Wind and Structures, Vol. 15, Issue 5, 2012, 385–407.
- [6] Gjelstrup H., Georgakis C.T., Larsen A., *A preliminary investigation of the hanger vibrations on the Great Belt East Bridge*, Proceedings of the 7th International Symposium on Cable Dynamics, Vienna 2007.

- [7] Górski P., Pospíšil S., Kuznetsov S., Tatara M., Marušić A., *Strouhal number of bridge cables with ice accretion at low flow turbulence*, Wind and Structures, Vol. 22, Issue 2, 2016, 253–272.
- [8] Hartog J.P.D., *Transmission-line vibration due to sleet*, Institute of Electrical Engineers, Vol. 51, 1932, 1074–1086.
- [9] Kuznetsov S., Pospíšil S., Král R., *Climatic wind tunnel for wind engineering tasks*, Technical Transactions, Vol. 12(2-B), 2015, 303–316.
- [10] Roldsgaard J.H., Kiremidjian A., Georgakis C.T., Faber M.H., *Preliminary probabilistic prediction of ice/snow accretion on stay cables based on meteorological variables*, Proceedings of the 11th International Conference on Structural Safety and Reliability, New York 2013.
- [11] Schewe G., *On the force fluctuations acting on a circular cylinder in crossflow from subcritical up to transcritical Reynolds numbers*, Journal of Fluid Mechanics, Vol. 133, 1983, 265–285.
- [12] Trush A., Pospíšil S., Kuznetsov S., Kozmar H., *Wind-tunnel experiments on vortex-induced vibration of rough bridge cables*, Journal of Bridge Engineering, Vol. 22, Issue 10, 2017, 1–8.



